A Hierarchical, Heterogeneous Material CAD Model with Application to Laser Sintering

David W. Rosen, Namin Jeong, Yan Wang
The George W. Woodruff School of Mechanical Engineering
Georgia Institute of Technology
Atlanta, GA 30332-0405

Variations in laser irradiance and local temperatures in laser sintering cause variations in porosity and material microstructure, which can affect mechanical properties of a part. From the design perspective, it is important to model microstructures, mechanical properties, and their relationships so that parts can be analyzed and designed taking into account their as-manufactured condition. In this paper, we propose the modeling of part geometry and microstructure by using a new hierarchical modeling method. A surfacelet transform is introduced to model microstructure. The application of image processing methods enables multi-resolution representations of microstructure. Combined with methods from computational materials design, low resolution microstructure representations can be used to compute effective mechanical properties. The models and methods are demonstrated on two examples, a simple fiber-reinforced composite and a laser sintered nylon-12 material.

1 INTRODUCTION

For many years, practitioners in the additive manufacturing (AM) industry have complained about the lack of suitable engineering materials. Others note the large variability and unpredictability of mechanical properties in AM processed materials. Both sets of users would benefit from computer-aided design (CAD) tools that integrate material information with geometry. Furthermore, the capability of deriving mechanical properties from the material and geometry information would greatly aid part design and engineering. In this paper, we present a new hierarchical, heterogeneous model for CAD that features multi-scale geometry and material information. The model is illustrated with examples of laser sintered (LS) nylon materials.

In multiscale CAD systems, ranging from nano (10^{-9}~10^{-8} m), meso (~10^{-7} m), micro (10^{-6}~10^{-4} m), to macroscales (>10^{-3} m), the specifications of material compositions and distributions are as important as geometric shapes. At the traditional macroscale in engineering design, geometry and materials can be separately specified. However, at the micro- and meso-scales, material compositions become important in functional realization, such as in composites and functionally graded materials. At the nano-scale, geometry and material property become one-to-one correspondent to each other, such as in crystals and metal-organic frameworks. Therefore, we need a concise and precise form to capture material compositions along with geometry so that engineers can design materials in an interactive environment.

Even though multi-resolution geometry representations (e.g., subdivision and wavelets) have been developed, the geometric information is only at the same length scale; from this information, representations at different levels of detail (LOD) can be generated. The major difference between *multiscale* and *multi-resolution* modeling is that in a multi-resolution environment, the complete model information is available at the highest resolution, while in multiscale modeling, the highest resolution need not be generated, except when and where it may

be needed. For instance, a multiscale model does not require the entire Boeing 787 airplane model to be available at the atomic scale if one component is required at this scale. Instead, in a multiscale environment, it is necessary to render the model at a specified scale when and where a specified region of a model can be rendered at a desired scale for a specific purpose, such as visualization, finite-element analysis, or manufacturing process planning [i].

In this paper, we propose a new multiscale geometric and materials modeling method that uses an implicit representation to efficiently capture internal and boundary information. This new approach can effectively represent multiscale complex structures as well as material compositions and distributions. It serves as the foundation for modeling structure-property relationships for materials design. We call our modeling approach *dual representation* or *dual-Rep*, since it represents both internal and boundary distributions of materials in a unified implicit form. This new model is proposed to support the multiscale zoom process. Fig. 1 illustrates how such a zoom process is important in representing multiscale materials such as bone structures. The external boundaries can be represented as continuous 2D red curves in Fig. 1a. As we zoom in, the zero-width boundary becomes a domain with internal material distributions, as in Fig. 1b. In other words, explicit boundaries with zero width in the previous scale now become continuous distributions of materials with fine-grained features inside the boundary structures themselves. On the other hand, when zoomed in, it becomes more convenient to model some internal regions where relatively high gradients of distributions exist (i.e., with large contrast between black and white colors in the images) by boundary representation, as in Fig. 1c. With further magnification of continuous regions to the atomic level, the polycrystalline structure emerges, where grain boundaries and defects can be modeled efficiently with boundary representations again, as in Fig. 1d. Therefore, boundary and internal are complementary structures. The purpose of the dual-Rep model is to support such role exchanges of boundary and internal structures at different length scales. The enabling core part of the dual-Rep model is a new basis function called surfacelet.

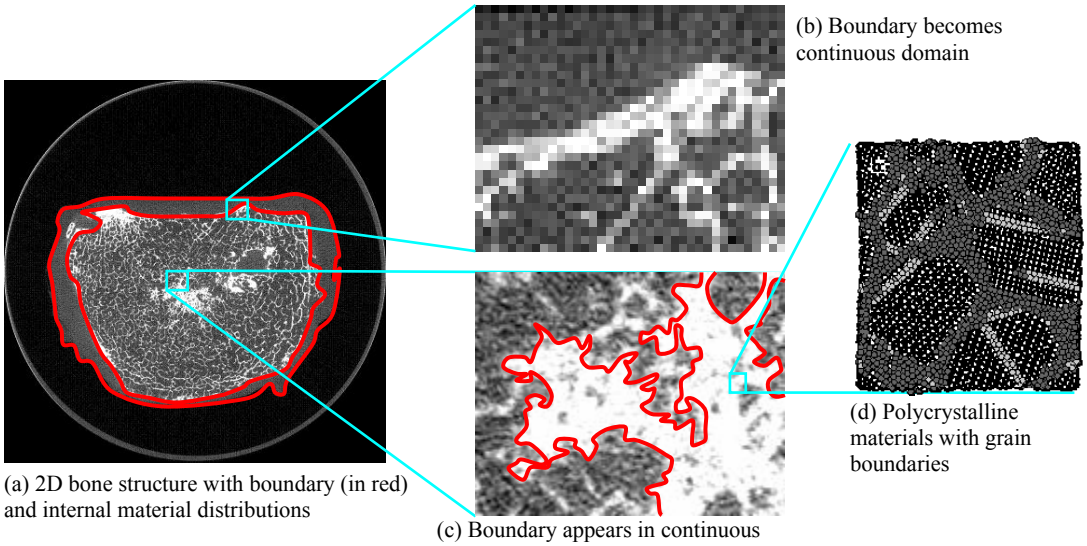

Fig. 1: An illustration of dual-Rep model for multiscale geometry and materials modeling with boundary and internal structures exchanges at difference scales.

In the remainder of the paper, we gave a brief background review of relevant work in Section 2. The proposed surfacelet functions are introduced in Section 3. The dual-Rep multiscale heterogeneous model based on surfacelet transforms is described in Section 4. In Sections 5 and 6, the surfacelet transform is applied to two example microstructures, a fiber-reinforced composite and a nylon-12 laser sintered material, to illustrate its multi-resolution capabilities.

2 BACKGROUND

In this section, we give a brief overview of relevant work to our proposed multiscale materials modeling approach, including heterogeneous modeling in Section 2.1 and multi-resolution geometry representations in Section 2.2.

2.1 Heterogeneous Modeling

Heterogeneous modeling usually denotes the modeling of geometry and material composition. Some researchers may include non-manifold topology under the term, which we allow, but do not emphasize. Two general approaches to heterogeneous modeling have been proposed [ii]: discretized and non-discretized approaches. In the first category, materials and geometry are modeled separately, such as mesh-based and voxel-based methods, where geometry is approximated by volume meshes or voxels [iii], and material distributions are determined by topology optimization or numerical interpolation from control features [iv]. Other researchers applied voxel-based representations that utilized spatial occupancy enumeration of part geometry [v]. General cellular decompositions have also received considerable attention [vi], including some with integrated physical property distributions model [vii]. Some researchers have generalized the cellular modeling approach to include manufacturing process-related Local Composition Control (LCC) elements [viii].

In non-discretized approaches, some researchers have separated the representation of material compositions and properties from the underlying part geometry [ix]. Others have utilized implicit modeling approaches, which has advantages in that a common mathematical model is used for both geometry and material composition [x]. Shapiro and coworkers have applied the theory of R-functions to show how material composition [xi] can be performed using implicit modeling approaches and extended the model to include distributions of any physically meaningful quantity throughout a part. A different group proposed a method based on hypertextures [xii] that provides more intuitive user controls, according to the developers.

The limitation of all work described here is that the models are not multiscale; at best some can be called multi-resolution, specifically the methods in the first general approach based on geometric decompositions. Even then, the resolutions are limited to the overall part geometry and the particular decomposition into cells, voxels, or mesh elements. In contrast, our proposed approach is both multiscale and multi-resolution, where part representations can be generated at the desired size scale and resolution.

2.2 Multi-resolution Geometry Representations

There have been various efforts on multi-resolution geometry representation. The basic ideas are based on functional approximations in the Hilbert space. Choosing appropriate basis functions that have multi-resolution properties is the core research issue. The most studied ones are B-splines and wavelets.

B-Spline: B-spline is widely used as the basis function in geometric modeling and simulation. Through knot insertion and degree elevation [xiii], B-spline curves and surfaces can be refined with more control points introduced. Reversely, control points can be reduced in approximations.

A more general multi-resolution representation is subdivision curves and surfaces [xiv, xv], which are based on the B-spline refinability. That is, the B-spline basis function can be written as a linear combination of the translated and dilated copies of itself. Therefore, by recursively refining control points based on some topological and geometric rules, the control polygon or mesh converges to the limit B-spline curve or surface.

Wavelets: In the domain of 2D shape representations, wavelets are among the most popular multi-resolution representations. Similar to Fourier analysis, wavelet analysis is to represent and approximate signals (or functions in general) with orthogonal or non-orthogonal basis functions. Both methods can be used to uncover frequency components of signals. Both can be used to represent multi-resolution subspaces and fast algorithms are available for both. However, instead of sinusoidal functions in Fourier analysis, the functional space for wavelet analysis is decomposed based on a scaling function $\varphi(t)$ and a wavelet function $\psi(t)$ with one dimensional variable t for multi-resolution analysis.

Wavelets are self-similar and can be scaled up and down. More specifically, the wavelet function

$$\psi_{a,b}(t) = a^{-1/2}\psi\left(a^{-1}(t-b)\right) \qquad (1)$$

is scaled by a scaling (dilation) factor *a* and translated by a translation factor *b*. Although certain forms (e.g. Haar, Daubechies, Morlet, etc.) have been used extensively, $\psi(t)$ is actually general and can be customized for specific problems. Similar operations can be applied to scaling functions. The most important feature of wavelets is that they are localized in both real (time) and reciprocal (frequency) spaces due to the property of regularity and vanishing moments. With these properties, wavelets together with scaling functions can be used to approximate signals and functions in a compact form (compared to the traditional Fourier analysis), with local features represented more efficiently. Wavelets provide a general approach for multi-resolution functional analysis. In geometric modeling domain, the wavelet transforms were used to describe planar curves with multiple resolutions [xvi].

The above different multi-resolution modeling approaches capture geometric information in different levels of detail. However, they do not meet the requirement of multiscale design scenarios, where geometric information as well as material properties should be captured in a way so that users can retrieve either low-granularity global structures or high-granularity local information without rendering the global picture with the greatest details.

Our proposed multiscale representation of geometry and materials is based on a hybrid approach of implicit and boundary representations. The general idea is to represent materials distribution in a domain and its boundary with a combination of two types of basis functions. While regular wavelets can be used in internal distributions, a new basis function is introduced to model materials distributions in boundaries, which is called *surfacelet*. It is a generalization of ridgelet and curvelet, as introduced in the next section.

Wedgelet, Curvelets, and Surflet: Wavelets perform well for objects with point singularities in dimension 1. However they are not effective in dealing with edge discontinuities in dimension 2.

Several so-called directional wavelet approaches have been proposed to solve this issue, including wedgelet [xvii], curvelet [xviii], and ridgelet [xix].

The wedgelet approach partitions 2D space into squares as building blocks which have line segments. 2D images then can be approximated by a collection of specifically chosen wedgelets. The curvelet function is an extension of the standard wavelet function, which combines the concepts of neural networks, Radon transform, and wavelets. It was developed to compress images containing continuous line or curve segments, where the standard wavelets are not efficient. The idea of the curvelet was originally started as ridgelet, where an angular element θ is introduced in the wavelet function as

$$\psi_{a,b,\theta}(\mathbf{r}) = \psi_{a,b}(x\cos\theta + y\sin\theta) = a^{-1/2}\psi\left(a^{-1}(x\cos\theta + y\sin\theta - b)\right) \qquad (2)$$

so that the parameters include scaling, translation, and orientation. Later, curvelet was constructed in the Fourier space in order to have better controls of resolution in the frequency domain. With the multi-resolution deployment of ridgelets, a parabolic scaling constraint of width $\approx$ length^2 can be introduced so that curvelets are no longer lines with infinite lengths. If wavelets can be thought of as "fat" points with certain widths of local support, curvelets are "fat" needles where orientation information can be captured.

In 3D analysis, Ying et al. [xx] extended 2D curvelet transform to 3D with similar frequency space tilings. Similarly, Lu and Do [xxi] extended contourlets to three dimensions in a discrete space. Chandrasekaran et al. [xxii] extended wedgelets to high-dimensional space and approximate functions with polynomial building blocks, called surflets, instead of linear building blocks in wedgelets.

In this paper, we propose a new modeling approach to capture multiscale material distributions with a new surfacelet basis function. The proposed surfacelet can be viewed as a 3D generalization of the above directional wavelets. Also different from the purpose of the above efforts, which is to develop efficient approaches to represent and compress edge and surface singularities in 2D or 3D images in the format of pixels or voxels, we are interested in modeling both continuous distributions and surface singularities efficiently in a unified implicit form. Our new surfacelet functions generalize the shape singularities to higher orders such as quadratic surfaces. This allows for more flexibilities of boundary representation. In contrast to the above directional wavelet bases which are constructed in the Fourier domain, we would like to have direct controls in Euclidean space. The surfacelet is described in Section 3.

In order to support dual-Rep that allows for multiscale materials representation, a mixture of wavelet and surfacelet basis functions is chosen. Wavelet basis functions are used for continuous distributions, whereas surfacelet basis functions are used for surface singularities or boundaries. This approach enables us to capture both internal and boundary domains in a unified form so that seamless zoom operations between scales can be performed.

3 SURFACELET

We need to represent both internal and boundary material distributions in multiscale and multi-resolution modeling. The exchange between boundaries and internal structures such as the ones in Fig. 1 cannot be captured efficiently in the forms of regular wavelets or splines. Therefore, a different approach is required. Boundaries can be viewed as surface singularities that are discontinuous in one direction while continuous in other two in 3D space. They can be

represented locally as planes, cylinders, ellipsoids, etc. Therefore, we propose surfacelet basis functions as building blocks of boundaries in multiscale modeling.

We define a general surfacelet basis function as

$$\psi_{a,b,\mathbf{p}}(\mathbf{r}) = a^{-1/2}\psi\left(a^{-1}\rho_{b,\mathbf{p}}(\mathbf{r})\right) \tag{3}$$

where $\mathbf{r} = (x, y, z)$ is the location in the domain Ω in the Euclidean space, $\psi : \mathbb{R} \to \mathbb{R}$ is a wavelet function, *a* is a non-negative scaling factor, $\rho_{b,\mathbf{p}} : \mathbb{R}^3 \to \mathbb{R}$ is a surface function so that $\rho_{b,\mathbf{p}}(x, y, z) = 0$ implicitly defines a surface, with the translation factor *b* and the shape parameter vector $\mathbf{p} \in \mathbb{R}^m$ determining the location and shape of surface singularities, respectively. Particularly, a 3D ridgelet that represents plane singularities is defined as

$$\psi_{a,b,\alpha,\beta}(\mathbf{r}) = a^{-1/2}\psi\left(a^{-1}(\cos\beta\cos\alpha \cdot x + \cos\beta\sin\alpha \cdot y + \sin\beta \cdot z - b)\right) \tag{4}$$

where $\alpha \in [0, 2\pi)$ and $\beta \in [-\pi/2, \pi/2]$ are angular parameters corresponding to rotations around z- and y-axes in the Euclidean space. Here the shape parameter vector is $\mathbf{p} = (\alpha, \beta)$. Similarly, a surfacelet that represents cylindrical singularities can be defined as

$$\psi_{a,b,\alpha,\beta,r_1,r_2}(\mathbf{r}) = a^{-1/2}\psi\left(a^{-1}\left[r_1(\cos\beta\cos\alpha \cdot x + \cos\beta\sin\alpha \cdot y + \sin\beta \cdot z - b)^2 + r_2(-\sin\alpha \cdot x + \cos\alpha \cdot y)^2\right]\right) \tag{5}$$

The isosurfaces of these two surfacelets for plane and cylindrical singularities are shown in Fig. 2, where the Mexican hat basis

$$\psi(t) = (2\pi)^{-1/2}\sigma^{-3}\left(1 - t^2\sigma^{-2}\right)e^{-t^2\sigma^{-2}/2} \tag{6}$$

is applied and $\sigma = 0.8$.

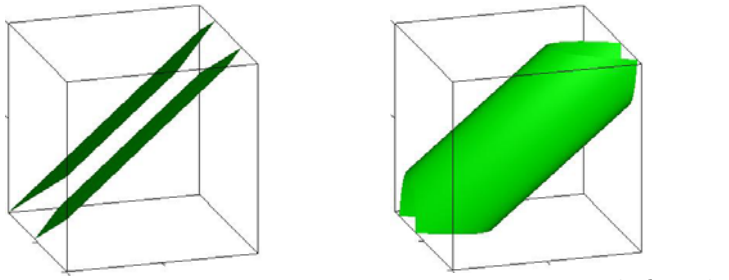

(a) 3D ridgelet ($a = 0.2$, $b = 0.1$, $\alpha = 11\pi/6$, $\beta = \pi/4$)

(b) Cylindrical surfacelet ($a = 0.2$, $b = 0.1$, $\alpha = 11\pi/6$, $\beta = \pi/4$, $r_1 = 1$, $r_2 = 4$)

Fig. 2: Isosurfaces of surfacelets.

The parameters of surfacelets can be geometrically interpreted as follows. For 3D ridgelets as in Fig. 3a, any point on a plane $\cos\beta\cos\alpha \cdot x + \cos\beta\sin\alpha \cdot y + \sin\beta \cdot z = t$ has the same evaluation of the wavelet function $\psi\left(a^{-1}(t - b)\right)$. Therefore, the isosurfaces of Eqn. 4 are planes. Similarly, for cylindrical surfacelets in Fig. 3b, all points on a cylinder

$r_1\left(\cos\beta\cos\alpha\cdot x+\cos\beta\sin\alpha\cdot y+\sin\beta\cdot z-b\right)^2+r_2\left(-\sin\alpha\cdot x+\cos\alpha\cdot y\right)^2=r_0^2$ have the same evaluation of wavelet functions in Eqn. 5.

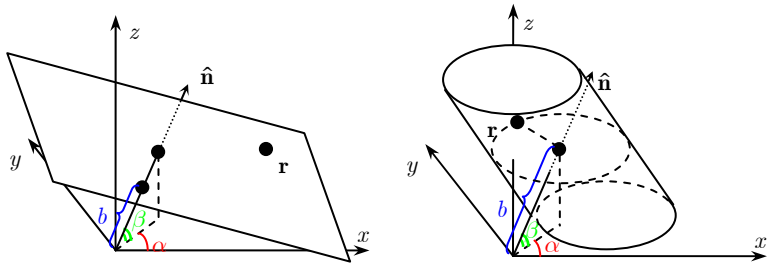

(a) 3D ridgelet (b) Cylindrical surfacelet

Fig. 3: Geometric interpretation of surfacelets.

4 DUAL-REP MULTISCALE HETEROGENEOUS MODEL

Based on the proposed surfacelet basis functions, we model complex and multiscale geometries in an implicit form for multi-materials representation and analysis. We are interested in modeling both internal and boundary distributions. As mentioned in Section 2.2, wavelets are efficient in representing one-dimensional point singularities but not two- or three-dimensional ones. In contrast, surfacelets are efficient in two- or three-dimensional singularities but not one-dimensional ones. Therefore, a combination of wavelet and surfacelet basis functions is chosen. Wavelet basis functions are used for continuous internal distributions, while surfacelet basis functions are used for boundary distributions.

In this paper, we will focus on the generation and manipulation of surfacelet models of laser sintered microstructure. In contrast, in an earlier paper [xxiii] we discussed the representation of material distributions and microstructures by first specifying materials and properties at a finite number of positions. Then the distributions within the domain can be interpolated based on selected basis functions.

The approach to generating surfacelet models of sintered microstructure can be described as reverse engineering of materials. We use nano- and micro-scale images such as those from atomic force microscopy and electron microscopy to characterize a material's structure. The boundaries of grains or phases can be detected from the images. In addition, the shading and its gradients in the images provide the information of material distributions. Given that calibration of images is done in the pre-processing step, a mapping from shading in images to properties can be achieved.

The Radon transform is an effective method for representing line singularities in 2D and 3D images [xxiv] (i.e., finding straight edges in images). The Radon transform was developed to reconstruct images from CT scans [xxv], which consist of sets of parallel scans where the source and sensor rotate around the target. We generate surfacelet models by first applying the Radon transform, or a Radon alike transform, to the image, to convert line or edge singularities to point singularities. Then, by applying a wavelet transform to the results of the Radon transform, a representation of the image can be produced that is potentially sparse and enables many image processing techniques to be applied. In our case, we want to take advantage of compression methods and the multi-resolution capabilities of wavelets.

Mathematically, the Radon transform in a domain Ω is the integral along the plane (represented as the dash line in 2D), which is perpendicular to a line at angle α, as illustrated in Fig. 4a. The plane and the line intersect at a point which has the radial distance of μ from the origin. Varying the radius μ results in a vector of integral values, $I_\alpha(\mu)$ in 2D and $I_{\alpha,\beta}(\mu)$ in 3D (in 3D, angles α and β. orient the lines along which the integrals are performed). That is,

$$I_\alpha(\mu) = \iint f(x,y)\,\delta(x\cos\alpha + y\sin\alpha - \mu)\,dxdy \qquad (7)$$

$$I_{\alpha,\beta}(\mu) = \iiint f(x,y,z)\,\delta(x\cos\beta\cos\alpha + y\cos\beta\sin\alpha + z\sin\beta - \mu)\,dxdydz$$

where δ is the Dirac delta function. The simplest surfacelet is the ridgelet transform, which is the 1D wavelet transform of the surface integral values $I_{\alpha,\beta}(\mu)$ on the plane as in

$$\Psi_{a,b,\alpha,\beta} = \left\langle I_{\alpha,\beta}(\mu), \psi_{a,b}(\mu) \right\rangle \qquad (8)$$

In general, our generic surfacelet transform is the 1D wavelet transform of the surface integrals. For the cylindrical surfacelet in Eqn.5, the surface integral is

$$I_{\alpha,\beta,r_0,r_1,r_2}(\mu) = \iiint f(x,y,z)\,\delta\begin{pmatrix} r_1(\cos\beta\cos\alpha\cdot x + \cos\beta\sin\alpha\cdot y + \sin\beta\cdot z - \mu)^2 \\ +r_2(-\sin\alpha\cdot x + \cos\alpha\cdot y)^2 - r_0^2 \end{pmatrix} dxdydz \qquad (9)$$

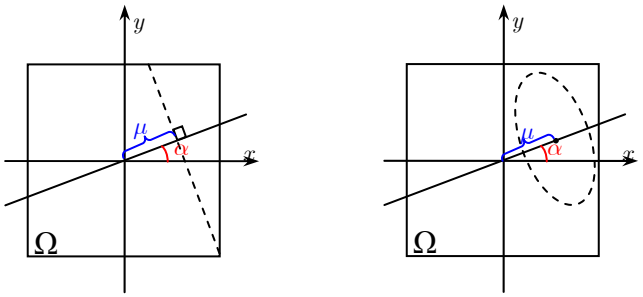

(a) ridgelet transform

(b) cylindrical and ellipsoidal surfacelets

Fig. 4: Geometric interpretations of parameters in surfacelet transforms.

We use the finite Radon and ridgelet transforms, as well as inverse transforms, from [xxiv] for our experiments. For a $p \times p$ image, the finite Radon transform is:

$$r_k(l) = \frac{1}{\sqrt{p}} \sum_{(i,j)\in L_{k,l}} f(i,j) \qquad (10)$$

where $f(i,j)$ is the pixel gray-scale value and $L_{k,l}$ denotes the set of points that make up a line on the lattice Z_p^2 ($Z_p = \{0,1,\ldots,p\text{-}1\}$):

$$L_{k,l} = \left\{(i,j) \;\middle|\; j = (ki + l) \bmod p, i \in Z_p\right\}$$
$$L_{p,l} = \left\{(l,j) \;\middle|\; j \in Z_p\right\} \qquad (11)$$

In this formulation, index k takes the place of angle α and l acts as distance μ.

The complete surfacelet transform is the result of applying the discrete wavelet transform to each slice (projection) of the Radon transform, which is each $r_k(l)$, for $l = 0,\ldots,p$. As a result, a materials model can be reconstructed from images based on the surfacelet transform defined by Eqns. 7-11. The process of computing surfacelet coefficients from 3D images is illustrated in Fig. 5. From a 2D materials distribution, the finite Radon transform is calculated and arranged in a 3D matrix with k and l as indices. Then 1D discrete wavelet transforms along the l axis direction are performed for all α's. The results are surfacelet coefficients for a particular angle.

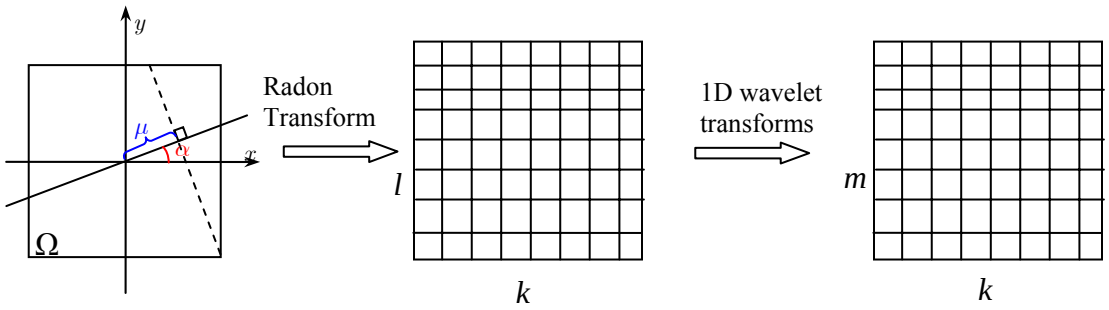

Fig. 5: The general process of surfacelet transforms.

5 SIMPLE FIBER-REINFORCED COMPOSITE EXAMPLE

The surfacelet representation and its hierarchical modeling capabilities are illustrated with a simple example of a fiber-reinforced composite material. Figure 6 shows the sample microstructure, with vertical and horizontal fibers spaced 100 μm apart. We assume a typical carbon-epoxy composite material with property values of $E_m = 2.94$ GPa, $E_{f1} = 234.6$ GPa, $E_{f2} = 13.8$ GPa. The sample's elastic modulus analytical model, surfacelet representation, 4X zoomed-out representation, and 4X zoomed-out elastic modulus model will be derived in this section.

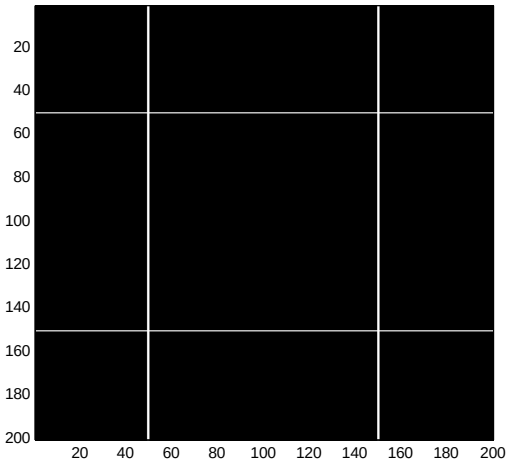

Fig. 6, Fiber-reinforced composite microstructure (dimensions in μm).

5.1 Elastic Modulus Model

The strain-stress relationship for this microstructure can be derived readily from basic composite materials models for a single fiber in a polymer matrix [xxvi]:

$$\varepsilon = \mathbf{S}\sigma = \begin{bmatrix} S_{11} & S_{12} & 0 \\ S_{12} & S_{22} & 0 \\ 0 & 0 & 2S_{66} \end{bmatrix} \begin{Bmatrix} \sigma_1 \\ \sigma_2 \\ \gamma_{12} \end{Bmatrix} \quad (12)$$

where the S_{ij} are four independent constants in the elastic compliance tensor of a unidirectional laminate in its local frame (E_m = elastic modulus of matrix, E_{fi} = elastic modulus of fiber in direction i, G = shear moduli, ν = Poisson's ratio, V_r = volume fraction of fiber):

$$S_{11} = \left(E_m\left(1-V_r\right)+E_{f1}V_r\right)^{-1} \qquad S_{22} = \frac{1-\sqrt{V_r}\left(1-E_m/E_{f2}\right)}{E_m} \tag{13}$$

$$S_{12} = \frac{\nu_m\left(1-V_r\right)+\nu_{f2}V_r}{E_m\left(1-V_r\right)+E_{f2}V_r} \qquad S_{66} = \frac{1-\sqrt{V_r}\left(1-G_m/G_{f12}\right)}{G_m}$$

5.2 Surfacelet Representation

The Radon transform of the microstructure is shown in Figure 7a, which illustrates the power of the transform for microstructures with linear elements. The four fibers from Fig. 6 are identified by the four bright spots (highlighted by manipulating the image) in the Radon transform at (k,l) = (0,61), (0,193), (130,61), and (130,193). The index values of k's here correspond to the angles of 0 and 90 degrees. Applying the biorthogonal spline wavelet (bior1.3 in the Matlab Wavelet Toolbox) to the Radon transform yields the surfacelet representation shown in Fig. 7b.

To view a macro-scale section of a part with this simple fiber-reinforced microstructure, the surfacelet representation can be compressed significantly, then reconstructed at a lower resolution. After eliminating 99.95 percent of the surfacelet coefficients from Fig. 7b, the zoomed-out surfacelet representation appears as in Fig. 7c. Fig. 7d shows the result after an inverse wavelet transform is performed, which corresponds to the Radon transform of the compressed microstructure. After performing the inverse finite Radon transform of Fig. 7d, we obtain the low resolution microstructure image shown in Fig. 7e, which is visually identical to the starting microstructure image. Its signal-to-noise ratio is 21.69 dB.

The most straight forward method of determining the zoomed-out mechanical properties of this microstructure is to utilize the rule of mixtures. Each pixel in Fig. 7e corresponds to a square section of material, with its gray-scale value representing its property value. For this example, each pixel will be assumed to have isotropic properties. As a result, the effective elastic modulus of the microstructure is given by

$$E_{eff} = \sum_{i=0}^{p-1}\sum_{j=0}^{p-1} v_r g_{ij}\left(E_f - E_m\right) + E_m$$

where v_r is the volume fraction of the pixel, g_{ij} is the gray-scale value of pixel i,j. After adjusting the gray-scale values relative to the original microstructure image by scaling the image size, the effective elastic modulus is 5.26 GPa, which compares favorably to the value of $C_{11} = S_{11}^{-1}$ that was computed using Eqn. 12 suitably modified to account for all four fibers, which was 7.4 GPa.

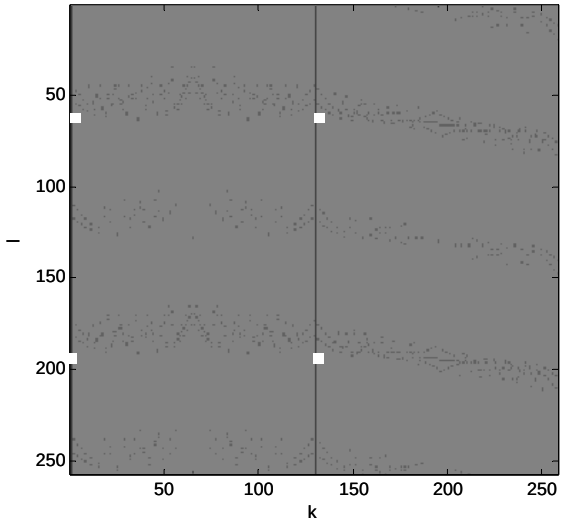

a. Radon transform

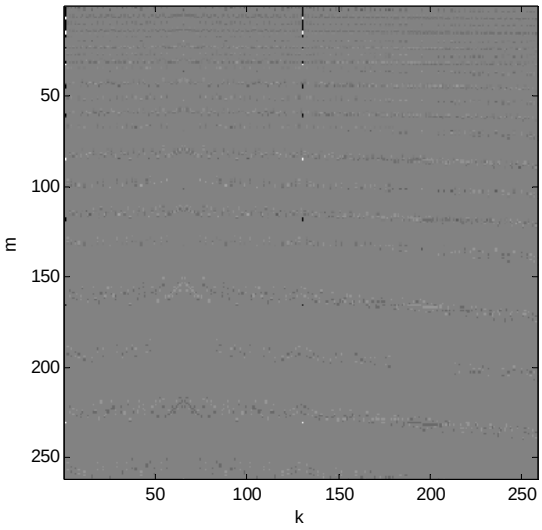

b. Surfacelet representation (discrete wavelet transform of (a)).

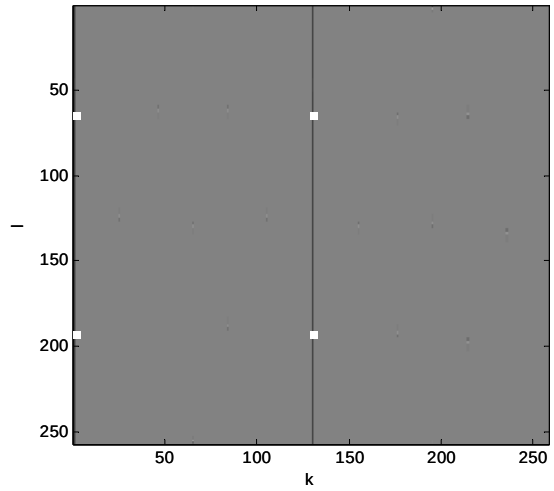

c. compressed (99.95%) surfacelet representation.

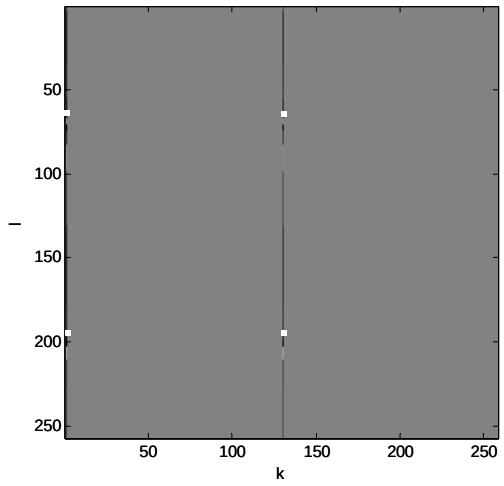

d. inverse wavelet transform (compare with (b)).

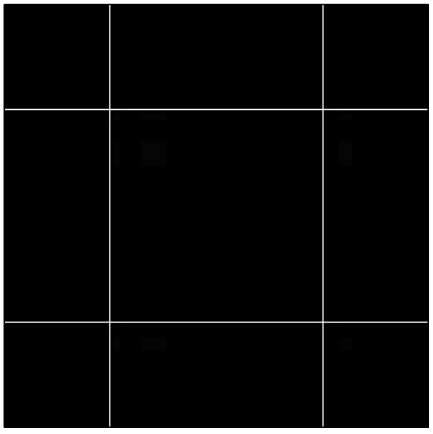

e. reconstructed compressed image.

Fig. 7. Fiber-reinforced composite example.

6 LASER SINTERED EXAMPLE

A section of laser sintered nylon-12 is shown in Figure 8a [xxvii], which will be the sample microstructure used for this example. Note the regions of symmetry in the x > 200 and y > 200 regions (used to increase the image size to be suitable for the finite Radon transform). In LS, it is common for powder particles to be partially melted, not fully melted. Partially melted regions are visible around the small dark clusters, which indicate unmelted particle cores. Regions with clear striations are fully melted areas and tend to have better mechanical properties. The large dark regions are assumed to have significant porosity.

Again, we are interested in assessing its elastic modulus at zoomed-out size scales. Similar to the previous example, we perform finite Radon (b) and wavelet (c) transforms, then compress the result of the wavelet transform (surfacelet representation) by 99 percent, as shown in Fig. 8d. The vertical white strips evident in Fig. 8b indicate directions along which a significant number of crystals (or other microstructure features) are oriented. In contrast, black regions indicate directions along which significant porosity occurs.

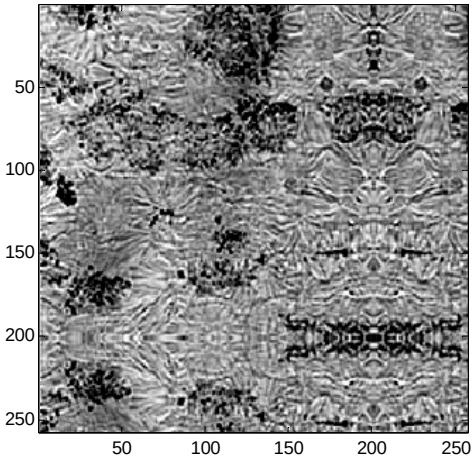

a. original microstructure image.

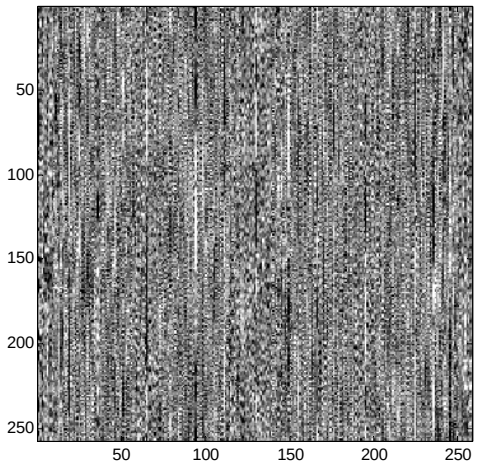

b. Radon transform of (a).

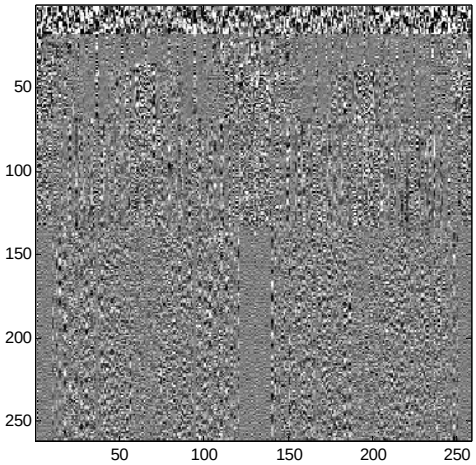

c. surfacelet representation.

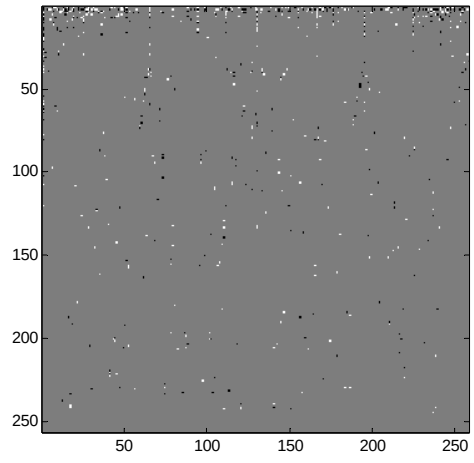

d. compressed surfacelet representation (99% compression).

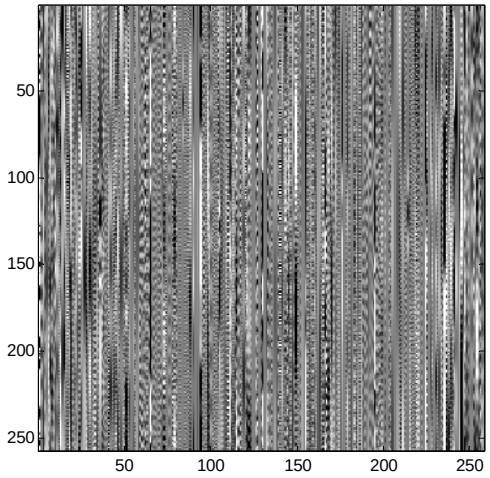

e. inverse wavelet transform (compare to (b)).

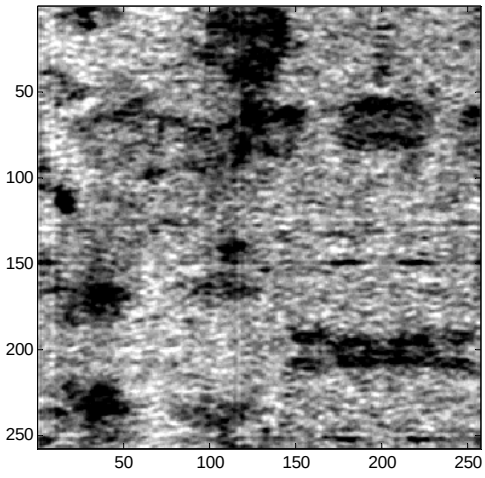

f. reconstructed microstructure image.

Fig. 8. Laser sintered material example.

Taking the inverse discrete wavelet transform of the compressed surfacelet yields Fig. 8e, which is significantly coarser than Fig. 8b, as we would expect. Yet, the compressed representation maintains enough information to reconstruct the microstructure, as seen in Fig. 8f.

The effective stiffness (C_{11}) of the compressed surfacelet can be determined in a manner similar to that used for the fiber-reinforced composite of Sec. 5. The gray-scale values in the image in Fig. 8e are used to indicate material types (porous, melted and oriented crystals, and unmelted cores) and their stiffnesses are combined to give the effective stiffness of the region in Fig. 8f. Dark regions in Fig. 8e correspond to porous nylon-12 (assumed C_{11} = 1200 MPa), bright regions correspond to oriented, melted material (assumed C_{11} = 2000 MPa, C_{22} = 1500 MPa), while intermediate regions correspond to unmelted and partially melted particles (assumed C_{11} = 1550 MPa). Computing the effective stiffness yields a value of 1600 MPa, which compares favorably with a measured tensile modulus value of approximately 1750 MPa [xxvii].

To illustrate the integration of a material model with part geometry, the compressed microstructure from Fig. 8f is applied to a section of a tensile test part, as shown in Fig. 9. The boundaries of a 5x5 mm section, including a curved region, were modeled using implicit geometry such that each boundary separates "inside" from "outside" the part. Boundary models were combined using an implicit intersection operator to

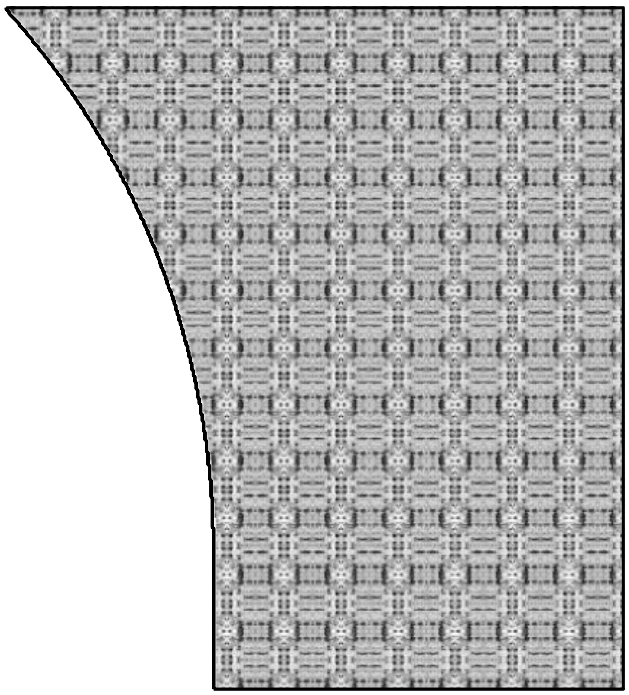

Fig. 9. 5x5 mm section of tensile bar with LS compressed microstructure.

yield an implicit function of the part section. Regions in the part interior have function values greater than 0, the part boundary has values of 0, and the region outside the part has function values less than 0. Then, the image in Fig. 8f is mapped into the interior of the part. X and Y mirror symmetries were used to tile the part interior in order to give a continuous looking microstructure.

7 SUMMARY

In this paper, we introduce a new hierarchical, heterogeneous representation, dual-Rep, to model both the geometry and material microstructure of parts. The dual-Rep model represents both internal and boundary distributions with a unified implicit form. Surfacelets as new basis functions are proposed to capture boundary information for both the part and the material microstructure (e.g., grain boundaries). A surfacelet model construction method was presented, based on a surfacelet transform, a 2-step process of computing a finite Radon transform, followed by a wavelet transform. Image processing methods were applied to generate lower resolution microstructure models. This particular surfacelet transform was effective in capturing linear microstructure features, such as crystal boundaries. Compression methods were applied to the surfacelet representation to significantly reduce the representation size, while still enabling microstructure reconstruction. Compression ratios of 99 percent and higher were demonstrated on a simple fiber-reinforced composite microstructure, as well as a laser sintered nylon-12 microstructure. Reasonable estimates of elastic modulus were computed from the compressed representations using rule-of-mixtures methods.

REFERENCES

[i] Rosen, D.W.: Thoughts on hierarchical modeling methods for complex structures, *Computer-Aided Design & Applications*, 6(3), 2009, 419-430.

[ii] Kou, X.Y.; Tan, S.T.: Heterogeneous object modeling: A review, *Computer-Aided Design*, 39(4), 2007, 284-301.

[iii] Bhashyam, S.; Shin, K.H.; Dutta, D.: An integrated CAD system for design of heterogeneous objects, *Rapid Prototyping Journal*, 6(2), 2000, 119-135.

[iv] Koenig, O.; Fadel, G.: Application of genetic algorithms in the design of multi-material structures manufactured in rapid prototyping, Proc. Solid Freeform Fabrication Symposium, pp. 209-217, Austin, TX, August 9-11, 1999.

[v] Wu, Z.W.; Soon, S. H.; Feng, L.: NURBS-based volume modeling, International Workshop on Volume Graphics, 321-330, 1999.

[vi] Adzhiev, V.; Kartasheva, E.; Kunii, T.; Pasko, A.; Schmitt, B.: Hybrid cellular-functional modeling of heterogeneous objects, *ASME Journal of Computing and Information Science in Engineering*, 2, 2002, 312-322.

[vii] Kumar, V.; Burns, D.; Dutta, D.; Hoffmann, C., "A framework for object modeling," *Computer-Aided Design*, 31, 1999, 541-556.

[viii] Liu, H.; Maekawa, T.; Patrikalakis, N.M.; Sachs, E.M.; Cho, W.: Methods for feature-based design of heterogeneous solids, *Computer-Aided Design*, 36, 2003, 1141-1159.

[ix] Tan, S.T.; Siu, Y.K.: Source-based heterogeneous solid modeling, *Computer-Aided Design*, 44(1), 2002, 41-55.

[x] Ganter, M.; Wahlborg, J.; Schwartz, D.; Storti, D.: H-ISM: An implementation of heterogeneous implicit solid modeling, Proc. ASME Design Automation Conference, paper #DETC2002/DAC-34139, Montreal, Sept 29 – Oct. 2, 2002.

[xi] Rvachev, V.L.; Sheiko, T.I.; Shapiro, V.; Tsukanov, I.: Transfinite interpolation over implicitly defined sets, *Computer Aided Geometric Design*, 18, 2001, 195-220.

[xii] Pratap, A.; Crawford, R.H.: Implementation of a functionally gradient material modeling and design system, Proc. Solid Freeform Fabrication Symposium, pp. 150-161, Austin, TX, Aug. 4-6, 2003.
[xiii] Piegl, L.; Tiller, W.: Software-engineering approach to degree elevation of B-spline curves, *Computer-Aided Design*, 26(1), 1994, 17-28.
[xiv] Catmull, E.; Clark, J.: Recursively generated B-spline surfaces on arbitrary topological meshes, *Computer-Aided Design*, 10, 1978, 350-355.
[xv] Doo, D.; Sabin, M.A.: Behaviour of recursive subdivision surfaces near extraordinary points, *Computer-Aided Design*, 10, 1978, 356-360.
[xvi] Daubechies, I.; Runborg. O.; Sweldens, W.: Normal multiresolution approximation of curve, *Constructive Approximation*, 20(3), 2004, 399-463.
[xvii] Donoho, D.: Wedgelets: nearly minimax estimation of edges, *The Annals of Statistics*, 27(3), 1999, 895-897.
[xviii] Candès, E.J.; Donoho, D.L.: Recovering edges in ill-posed inverse problems: optimality of curvelet frames, *The Annals of Statistics*, 30(3), 2002, 784-842.
[xix] Candès, E.J.: Ridgelets: theory and applications. Ph.D. dissertation, Standford University, 1998.
[xx] Ying, L.; Demanet, L.; Candès, E.: 3D discrete curvelet transform, Proc. SPIE Conf. Wavelet Applications in Signal & Image Processing, San Diego, CA, vol. 5914, pp.591413, 2005.
[xxi] Lu, Y.M.; Do, M.N.: Multidimensional directional filter banks and surfacelets, *IEEE Transactions on Image Processing*, 16(4), 2007, 918-931.
[xxii] Chandrasekaran, V.; Wakin, M.B.; Baron, D.; Baraniuk, R.G.: Representation and compression of multidimensional piecewise functions using surflets, *IEEE Transactions on Information Theory*, 55(1), 2009, 374-400.
[xxiii] Wang, Y., Rosen, D.W., "Multiscale Heterogeneous Modeling with Surfacelets," *Computer-Aided Design & Applications*, 7(5):759-776, 2010.
[xxiv] Do, M.N., Vetterli, M., "The Finite Ridgelet Transform for Image Representation," *IEEE Trans. Image Processing*, **12**(1):16-28, 2003.
[xxv] Kak, A.C., Slaney, M., *Principles of Computerized Tomographic Imaging*, SIAM, 2001.
[xxvi] Chamis, C.C., "Mechanics of Composite Materials: Past, Present, and Future," *Journal of Composites Technology and Research*, **11**(1):3-14, 1989.
[xxvii] Zarringhalam, H., Hopkinson, M., Kamperman, N.F., de Vlieger, J.J., "Effects of Processing on Microstructure and Properties of SLS Nylon 12," *Materials Science & Engineering A*, **435-436**: 172-180, 2006.